2D Linear Oculomotor Plant Mathematical Model: Verification and Biometric Applications

OLEG KOMOGORTSEV, COREY HOLLAND, SAMPATH JAYARATHNA, ALEX KARPOV, Texas State University

This paper assesses the ability of a two-dimensional linear homeomorphic oculomotor plant mathematical model to simulate normal human saccades on a two-dimensional plane. The proposed model is driven by a simplified pulse-step neuronal control signal and makes use of linear simplifications to account for the unique characteristics of the eye globe an the extraocular muscles responsible for horizontal and vertical eye movement. The linear nature of the model sacrifices some anatomical accuracy for computational speed and analytic tractability, and may be implemented as two one-dimensional models for parallel signal simulation. Practical applications of the model might include: improved noise reduction and signal recovery facilities for eye tracking systems; additional metrics from which to determine user effort during usability testing; and enhanced security in biometric identification systems. The results indicate that the model is capable of produce oblique saccades with properties resembling those of normal human saccades, and is capable of deriving muscle constants that are viable as biometric indicators. Therefore, we conclude that sacrifice in the anatomical accuracy of the model produces negligible effects on the accuracy of saccadic simulation on a 2D plane, and may provide a usable model for applications in computer science, human-computer interaction, and related fields.

Categories and Subject Descriptors: **I.2.10 [Artificial Intelligence]**: Vision and Scene Understanding—*Modeling and recovery of physical attributes*; **I.5.1 [Pattern Recognition]**: Models—*Structural*; **I.6.4 [Simulation and Modeling]**: Model Validation and Analysis

General Terms: Verification

Additional Key Words and Phrases: Human visual system, biological system modeling, mathematical model, biometrics.

ACM Reference Format:

Komogortsev, O., Holland, C., Jayarathna, S., and Karpov A. 2013. 2D Linear Oculomotor Plant Mathematical Model: Verification and Biometric Applications. ACM Trans. Appl. Percept. X, Y, Article Z (May 2013), 13 pages.

DOI=10.1145/0000000.0000000

1. INTRODUCTION

The human oculomotor plant (OP) consists of the eye globe and six extraocular muscles (EOM), the medial rectus, lateral rectus, superior rectus, inferior rectus, superior oblique, and inferior oblique. The OP, driven by a neuronal control signal, exhibits six primary types of eye movement: fixation, saccade, smooth pursuit, optokinetic reflex, vestibular-ocular reflex, and vergence (Leigh and Zee 2006). Each EOM is represented by a complex anatomical structure consisting of components that can be considered abstractly through such properties as series elasticity, viscosity, active-state tension, length-tension, and force-velocity relationships.

The physical and neurological characteristics of human eye movements have been a major subject of interest for medical professionals for well over a century, being a simplified basis from which to expand knowledge of similar muscular systems (Collins 1975). In recent years, a number of models have been proposed by various sources (Bahill 1980, Clark and Stark 1974, Enderle and Zhou 2010, Komogortsev and Khan 2008, Komogortsev and Khan 2009, Martin and Schovanec 1998, Robinson 1973, Westheimer 1954) for the oculomotor plant and its corresponding neuronal control signal, generally representing the oculomotor plant linearly in one-dimension (horizontal) or non-linearly in three-dimensions (horizontal, vertical, torsional) (Quaia and Optican 2003). Linear one-dimensional models have thus far failed to reproduce the saccadic trajectories and amplitude-peak velocity relationships present in normal human saccades, while non-linear three-dimensional models have received limited testing and are computationally complex, making them less suitable for real-time application.

Special gratitude is expressed to Dr. Christian Quaia for his comments and suggestions, and Katie J. Holland for her aid with technical illustrations. This work is supported in part by NSF CAREER Grant #CNS-1250718 and NSF GRFP Grant #DGE-11444666, and NIST Grants #60NANB10D213 and #60NANB12D234.

Author's address: O. Komogortsev, Texas State University, Department of Computer Science, San Marcos, TX 78666; email: ok11@txstate.edu; C. Holland, Texas State University, Department of Computer Science, San Marcos, TX 78666; email: ch1570@txstate.edu; S. Jayarathna, Texas A&M University, Department of Computer Science & Engineering, College Station, TX 77843; email: uksjayarathna@tamu.edu; A. Karpov, Texas State University, Department of Computer Science, San Marcos, TX 78666; email: ak26@txstate.edu.

DOI10.1145/0000000.0000000

The two-dimensional oculomotor plant mathematical model (2D-OP) considered in this paper builds on the one-dimensional OP model developed by (Komogortsev and Khan 2008), and provides the ability to simulate saccadic trajectories with supplied amplitude and onset position. The 2D-OP incorporates several important characteristics of the human oculomotor plant: each EOM is modeled individually, maintaining physiological agonist-antagonist dynamics; the model of each EOM encapsulates series elasticity, length-tension, viscosity, active-state tension, and force-velocity relationships; the model is driven by a pulse-step neuronal control signal, sent by the brain to the EOMs. The 2D-OP relies on a number of simplifications, representing a non-linear three-dimensional system as a linear two-dimensional system, sacrificing some amount of realistic accuracy (negligible due to the scale) for computational efficiency and analytic tractability.

In this paper, we assess the ability of the two-dimensional linear homeomorphic oculomotor plant mathematical model to simulate normal human saccades on a two-dimensional plane. In doing so, we investigate several connected issues concerning the viability of the 2D-OP for applications in computer science, human-computer interaction, and related fields, specifically: the ability of the 2D-OP to simulate oblique saccades with properties resembling those of normal human saccades; the physiological accuracy of component parameters required for such application; and the precision of parameters derived for person-specific saccades. As well, we provide an analysis of anatomical simplifications employed by the 2D-OP and their impact on saccadic simulation.

2. HUMAN VISUAL SYSTEM

2.1 The Oculomotor Plant

The human oculomotor plant, shown in Figure 1 with model comparison in Figure 2, consists of the eye globe and six extraocular muscles, the lateral rectus, medial rectus, superior rectus, inferior rectus, superior oblique, and inferior oblique. The lateral and medial recti are primarily responsible for horizontal rotation, the superior and inferior recti are primarily responsible for vertical rotation, and the superior and inferior oblique are responsible for torsional rotation of the eye globe.

Each muscle is represented by a complex anatomical structure, the properties of which can be effectively described by: ***series elasticity*** – the elastic resistance to rapid changes in muscle length produced by active muscles; ***passive elasticity*** – the elastic resistance to rapid changes in muscle length produced by inactive muscles; ***length-tension relationship*** – the relationship between the length of a muscle and the force it is capable of exerting during activation; ***force-velocity relationship*** – the relationship between the velocity of muscle contraction/relaxation and the force it is capable of exerting; ***active-state tension*** – the tension developed as a result of muscle activation by the neuronal control signal. As well, the eye globe and surrounding tissue display passive elastic and viscous properties.

2.2 The Brainstem Control

The brainstem control involves a neuronal control signal, generated by the brain and sent to the individual extraocular muscles, is responsible for the muscle contractions and relaxations that produce the many and varied types of human eye movement. According to Sherrington's law of reciprocal innervation (Ciuffreda and Stark 1975), the neuronal control signal is generated and sent to opposing muscles simultaneously, such that when an agonist muscle contracts, the opposing antagonist muscle relaxes. Further, the neural signals which control horizontal and vertical eye movements are generated in different regions of the brain; specifically, the neuronal control signal responsible for activation of the lateral and medial recti is generated in the paramedian pontine and medullary reticular formations, while the neuronal control signal responsible for activation of the superior and inferior recti is generated in the medial longitudinal fasciculus (Leigh and Zee 2006).

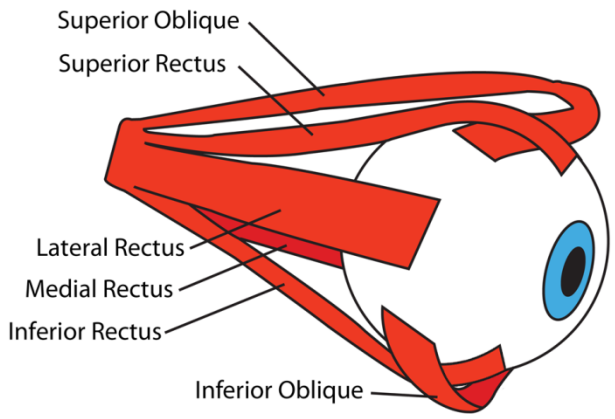

Figure 1. The Oculomotor Plant.

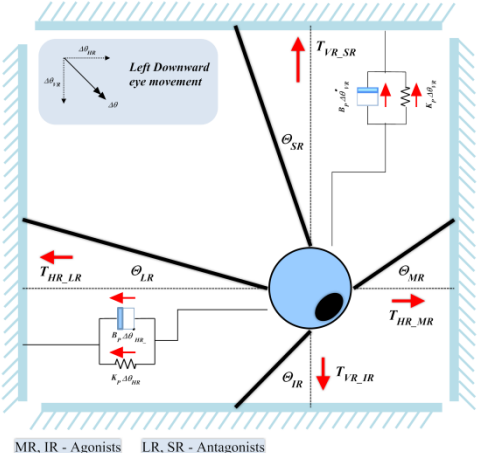

Figure 2. The Oculomotor Plant Model.

2.3 Eye Movements

Among the various eye movement types exhibited by the human visual system, fixations, saccades, and smooth pursuits are of particular interest. Fixations occur when the eye globe is held in a relatively stable position such that the fovea remains centered on an object of interest, providing heightened visual acuity; saccades occur when the eye globe rotates quickly between points of fixation, with very little visual acuity being maintained during rotation; and smooth pursuits occur when the eye globe rotates relatively slowly to maintain visual acuity on an object moving within the visual field. Saccades provide an ideal medium through which to study both the physical and neurological components of the oculomotor plant, due to their stereotyped behavior and the ease with which they can be reproduced by simple stimuli.

Saccades of given amplitude produced by an individual tend to show similarities in a number of properties, including: reaction time, duration, velocity, acceleration, and waveform. As well, certain relationships exist between saccades of varying amplitudes, these include: the amplitude-peak velocity relationship, the amplitude-duration relationship, and the velocity waveform.

The amplitude-peak velocity relationship (Bahill, et al. 1975), also referred to as the main sequence relationship, describes the tendency for saccadic peak velocity (V_{PEAK}) to increase with amplitude (A) in an exponential manner until saturation begins to occur at a certain velocity maximum (V_{MAX}), with curvature described by a constant (C_1), according to (1):

$$V_{PEAK} = V_{MAX} \times (1 - e^{-|A| / C1}) \tag{1}$$

The amplitude-duration relationship (Carpenter 1977) describes the tendency for saccade duration (D) to increase linearly with amplitude (A) from a base duration (D_{MIN}), with slope described by a constant (C_2), following (2):

$$D = D_{MIN} + C_2 \times |A| \tag{2}$$

The main sequence and amplitude-duration relationships vary by angle of motion, with differences in the relationships exhibited by horizontal, vertical, and oblique saccades. While there has been considerable research into these relationships as they relate to purely horizontal and vertical saccades, there is relatively little information on oblique saccades. In addition, these relationships have been noted to vary between individuals and may be affected by subject age (Fioravanti, et al. 1995, Huaman and Sharpe 1993), recording medium (Yee, et al. 1985), and initial eye position (Pelisson and Prablanc 1988). The velocity waveform is another characteristic that remains similar across saccades of varying amplitudes (Leigh and Zee 2006). It has been noted that the ratio of peak velocity to average velocity (Q) remains nearly constant at 1.6 for horizontal and vertical saccades of all amplitudes.

Given the fact that the horizontal and vertical components of human saccades are generated by separate areas of the brain and display noted differences in duration and peak velocity, oblique trajectories should be curved when component durations are unequal (Harwood and Herman 2008). While a substantial percentage of oblique saccades do exhibit curved trajectories, similarly substantial percentages exhibit trajectories that are near straight, more so than could be explained by the random synchronization of component duration (Bahill and Stark 1977).

Based on the frequent occurrence of straight oblique trajectories, it is apparent that the neural signals responsible for the horizontal and vertical components of oblique saccades in some way influence each other. Whether component stretching occurs before or after generation of the neuronal control signal is an area of active research (Sparks 2002). To simplify the analysis of our model, we assume that the duration of both components of movement is equal.

3. OCULOMOTOR PLANT MODEL

3.1 Description & Equations

One of the objectives of the oculomotor plant model presented in this paper is to accurately simulate saccade trajectories on the 2D plane. According to Table 9-2, p. 388 (Leigh and Zee 2006), the rotation of the eye globe, with mapped gaze position, on a two-dimensional plane can be primarily attributed to four extraocular muscles – the lateral, medial, superior, and inferior recti. Based on this information, we simplify the model by not explicitly including the contribution of oblique muscles. Figure 2 illustrates the extraocular muscle forces (T_{LR}, T_{MR}, T_{SR}, and T_{IR}) responsible for left-downward rotation ($\Delta\theta$) of the eye globe. Each muscle in the diagram is a simplified Hill-type muscle described in detail by (Komogortsev 2007, Komogortsev and Khan 2008, Komogortsev and Khan 2009).

During two-dimensional eye movement, the dynamics and roles of the extraocular muscles remain essentially the same as in one-dimensional movement. That is, the agonist muscles contract and pull the eye globe in the required direction, while the antagonist muscles stretch and resist the pull. Detailed mechanics of one-dimensional horizontal movement were previously described in detail by (Komogortsev 2007, Komogortsev and Khan 2008, Komogortsev and Khan 2009). The torsional component of movement is not included in the 2D-OP model, allowing application of the same logic for modeling both components of movement.

As a result, to simulate two-dimensional movement ($\Delta\theta$), all participating vector forces can be effectively projected into horizontal and vertical component forces, the computation of which includes the horizontal ($\Delta\theta_{HR}$) and vertical ($\Delta\theta_{VR}$) components of $\Delta\theta$. Projected force components are exactly the same as their one-dimensional counterparts, thereby allowing the simulation of $\Delta\theta_{HR}$ and $\Delta\theta_{VR}$ by equations (17) – (26) of (Komogortsev and Khan 2008). Then, the two-dimensional oculomotor plant mathematical model can be represented by a combination of two one-dimensional oculomotor plant models described by (Komogortsev 2007, Komogortsev and Khan 2008, Komogortsev and Khan 2009) and represented by (3) and (4):

$$\dot{x} = Ax + b \tag{3}$$

$$\dot{y} = Ay + b \tag{4}$$

Following Figure 3, (3) represents the system of equations necessary to simulate the horizontal component of movement, (4) represents the system of equations necessary to simulate the vertical component of movement, and state vectors x and y take the form of w. Model parameters include: elapsed time (Δt), series elasticity (K_{SE}), passive elasticity (K_P), length tension (K_{LT}), viscosity (B_P), force-velocity relationships (B), eye globe inertial mass (J), activation time constants (τ), and neural pulse (N). State variables include: eye position ($\Delta\theta$), eye velocity ($\Delta\theta$), length-tension displacement ($\Delta\theta_{LT}$), and active-state tension (F). Subscripts: DIM indicates the direction of movement; EOM indicates the agonist or antagonist muscle value for the lateral/superior recti of the right eye, or the medial/superior recti of the left eye; XOM indicates the agonist or antagonist muscle value for the medial/inferior recti of the right eye, or the lateral/inferior recti of the left eye; AG indicates agonist muscle values; ANT indicates antagonist muscle values. In their full form, (3) and (4) are defined by 36 parameters with values and relevant sources outlined in Sections 4 and 5.

3.2 Simplifications & Justification

The 2D-OP is not an exact replica of the human oculomotor plant and employs a number of simplifications to facilitate modeling, these include: neglect for the effects of the superior and inferior oblique muscles; linear representation of typically non-linear anatomical components (Quaia, et al. 2010); and three-dimensional rotations modeled as two-dimensional translations. Model simplifications, while substantial, are considered acceptable for its intended applications in the fields of computer science and human-computer interaction (Enderle, et al. 1991).

The superior and inferior oblique muscles are not modeled explicitly by the 2D-OP as they are primarily responsible for torsional rotation of the eye globe, and their effect on the two-dimensional plane is largely in the form of passive resistance. Linear representation of typically non-linear components (notably the force-velocity relationship) is the greatest source of anatomical inaccuracy; however, this is a simplification employed by many one-dimensional models and considered acceptable due primarily to the minute scale. Modeling of three-dimensional rotations as two-dimensional translations is acceptable for saccades to secondary positions, again due to scale, but neglects the non-commutativity of rotations when modeling saccades to tertiary positions (Tweed and Vilis 1987).

$$A = \begin{bmatrix} 1 & 0 & 0 & \Delta t & 0 & 0 \\ \frac{\Delta t\, K_{SE}^2}{B_{EOM}(K_{SE}+K_{LT})} & 1 - \frac{\Delta t\, K_{SE}}{B_{EOM}} & 0 & 0 & \frac{\Delta t\, K_{SE}}{B_{EOM}(K_{SE}+K_{LT})} & 0 \\ \frac{\Delta t\, K_{SE}^2}{B_{XOM}(K_{SE}+K_{LT})} & 0 & 1 - \frac{\Delta t\, K_{SE}}{B_{XOM}} & 0 & 0 & \frac{-\Delta t\, K_{SE}}{B_{XOM}(K_{SE}+K_{LT})} \\ \frac{-\Delta t(2K_{SE}+K_P)}{J} & \frac{\Delta t\, K_{SE}}{J} & \frac{\Delta t\, K_{SE}}{J} & 1 - \frac{\Delta t\, B_P}{J} & 0 & 0 \\ 0 & 0 & 0 & 0 & 1 - \frac{\Delta t}{\tau_{EOM}} & 0 \\ 0 & 0 & 0 & 0 & 0 & 1 - \frac{\Delta t}{\tau_{XOM}} \end{bmatrix} \quad b = \begin{bmatrix} 0 \\ 0 \\ 0 \\ 0 \\ \frac{\Delta t\, N_{EOM}}{\tau_{EOM}} \\ \frac{\Delta t\, N_{XOM}}{\tau_{XOM}} \end{bmatrix} \quad w = \begin{bmatrix} \Delta\theta_{DIM} \\ \Delta\theta_{LT\_EOM} \\ \Delta\theta_{LT\_XOM} \\ \Delta\dot{\theta}_{DIM} \\ F_{EOM} \\ F_{XOM} \end{bmatrix}$$

Figure 3. Two-Dimensional Linear Homeomorphic Oculomotor Plant Mathematical Model Equations.

3.3 Benefits & Applications

The 2D-OP, however simplified, represents the major anatomical components of the human oculomotor plant. The 2D-OP allows simulation of saccade trajectories in cases where amplitude and onset position are provided to the model. According to (3) and (4), the 2D-OP is essentially represented by two separate 1D-OP models, coinciding with the separation of those components in the brain, as discussed in Section 2.2. Computationally this solution is attractive, as separate cores of multi-core systems can compute both components of movement.

Practical applications of the 2D-OP may include: biometric systems, in which individual anatomical components represented by the 2D-OP allow for the unique identification of individuals (Komogortsev, et al. 2012b); human-computer interaction, in which simulated saccadic trajectories allow research into the properties of the eye movement signal, providing the capability for developing extremely fast target selection methods, in which selection occurs at saccade onset (Komogortsev, et al. 2009); usability, in which individual extraocular muscle forces can be approximated by the 2D-OP, providing an opportunity to estimate the physical effort exerted by a user during a specific task (Tamir, et al. 2008); eye tracking, in which the linear design of the 2D-OP allows its encapsulation in Kalman filter form, providing the means for robust signal recovery, noise reduction, and saccade predication for gaze-contingent compression (Komogortsev and Khan 2007, Komogortsev and Khan 2008).

4. METHODOLOGY

4.1 Participants

Eye movement recordings were collected for 30 subjects (24 male and 6 female), ages 18-40 with average age of 23 (SD = 5.3). For consistency, all recordings were generated for the right eye. The Texas State University Institutional Review Board approved data collection procedures and all subjects provided informed consent.

4.2 Apparatus & Software

Eye movement were recorded using an EyeLink 1000 eye tracking system running at 1000Hz with an average calibration accuracy of 1.31° (SD = 0.88°). A chinrest was employed to improve eye tracking accuracy, and subjects were positioned such that the primary eye position corresponded to the center of the screen. Stimuli were presented on a flat screen monitor positioned at a distance of approximately 695 millimeters from the subject, with screen dimensions of 640 × 400 millimeters and a screen resolution of 2560 × 1600 pixels. Algorithms and data analysis were implemented and performed in MATLAB.

4.3 Procedure

The screen was divided into four Cartesian quadrants, with the center of the screen as the origin. Eye movement recordings were generated under two experiment paradigms. In both cases, saccades were evoked by a white jumping-dot stimulus on a black background, and each stimulus point was displayed for 1000 milliseconds.

For the first experiment paradigm, recordings were generated for centrifugal saccades at different angles within the 1st quadrant (upper-right) of the screen. Due to screen dimensions, stimuli evoked saccades of 3°, 6°, 9°, 12°, 15°, and 18° amplitude at oblique angles of 0°, 15°, 30°, 45°, and 60°, and stimuli evoked saccades of 3°, 6°, 9°, 12°, and 15° amplitude at oblique angles of 75° and 90°. This resulted in a total of 40 stimulus-evoked oblique saccades per recording, for 1200 saccades across all subjects. A stimulus was presented at the origin before each saccade, and the order of stimulus presentation was randomized for each subject according to a uniform distribution.

For the second experiment paradigm, recordings were generated for random saccades across the screen. This allowed a high degree of variability in the saccades produced by each subject. 100 stimulus-evoked oblique saccades were generated per recording, with 4 recordings per subject, for 400 saccades per subject and 12000 saccades across all subjects. Stimuli were separated by a minimum of 2° amplitude, the stimulus was not restricted to centrifugal saccades, and the order of stimulus presentation was randomized for each subject according to a uniform distribution.

4.4 Processing

Eye movement recordings were processed to identify fixations and saccades. A velocity threshold algorithm (I-VT) (Komogortsev, et al. 2010) classified individual points with a velocity greater than 25°/sec as saccades, where all remaining points were assumed to be fixations, a micro-saccade filter re-classified saccades with amplitude less than 0.25° as fixations, and a micro-fixation filter re-classified fixations with a duration less than 50 milliseconds as saccades.

To investigate the ability of the 2D-OP to simulate oblique saccades with properties resembling those of normal human saccades, an optimization problem was defined to reduce the sum of absolute positional error between measured and simulated saccades. That is, Error = $\Sigma |m_i - s_i|$, where m_i is the measured position at a given time, i, and s_i is the simulated position produced by the 2D-OP model.

OPC for the horizontal and vertical trajectory of each saccade were optimized separately, according to Algorithm 1, and all model parameters were allowed to vary, these include (with initial values, based on measured physiological values): $K_{SE\_AG} = 2.5$, $K_{SE\_ANT} = 2.5$, $K_{LT\_AG} = 1.2$, $K_{LT\_ANT} = 1.2$, $N_{AG\_C} = 0.8$, $N_{ANT\_C} = 0.3$, $N_{FIX\_C} = 14.0$, $B_P = 0.06$, $B_{AG} = 0.046$, $B_{ANT} = 0.022$, $J = 0.000046$, $\tau_{AG\_AC} = 11.7$, $\tau_{ANT\_AC} = 2.4$, $\tau_{AG\_DE} = 2.0$, $\tau_{ANT\_DE} = 1.9$, $N_{AG\_SAC} = 100.0$, $N_{ANT\_SAC} = 0.5$, and PW_{AG} for each component; where $K_P = N_{AG\_C} - N_{ANT\_C}$ in all relevant equations. Optimization was performed across all possible pulse widths within the duration of a given saccade using the Nelder-Mead (NM) simplex search algorithm (Lagarias, et al. 1998) (MATLAB's fminsearch implementation) to minimize the absolute positional error between the measured and simulated trajectory. The pulse width with the least-error OPC set was selected for each saccade component. This resulted in the optimization of 18 OPC per component of each saccade, or 36 OPC to describe each saccade.

For the first experiment paradigm, stimulus-evoked centrifugal saccades were extracted from the recordings according to the following criteria: the saccade occurred between 100 and 500 milliseconds after the stimulus was displayed; the saccade had duration between 10 and 200 milliseconds; and at least one component of the saccade had positive amplitude. Only centrifugal saccades were considered, as it has been found that centrifugal/centripetal saccades often exhibit different dynamics. By filtering saccades in this manner, the algorithm was able to identify an average of 38 (SD = 2.1) stimulus-evoked saccades per recording. Across all subjects, 1140 of the possible 1200 stimulus-evoked saccades were identified.

For the second experiment paradigm, targeting investigation of the biometric potential of the model, we use all saccades identified within each recording, with horizontal and vertical saccade components considered separately. That is, the horizontal component of an oblique saccade was analyzed without consideration for its vertical component, and vice versa. Without additional filtering, an average of 75 (SD = 8.8) horizontal saccades and an average of 69 (SD = 15.2) vertical saccades were identified per recording, with a total of 9005 horizontal saccades and 8246 vertical saccades identified across all recordings.

Algorithm 1. OPC Estimation

1. Perform optimization of all OPC across all pulse widths for each saccade using NM to minimize the absolute positional error between the measured and simulated trajectory. This generates an OPC set for each possible pulse width of each saccade.
2. Select initial 3 least-error OPC sets for each saccade.
3. For each subject, average and fix the least-error values of the following model OPC across all saccades: K_{SE_AG}, K_{SE_ANT}, K_{LT_AG}, K_{LT_ANT}, N_{AG_C}, N_{ANT_C}, B_P, B_{AG}, B_{ANT}, J, τ_{ANT_AC}, τ_{AG_DE}, τ_{ANT_DE}, N_{FIX_C}, N_{ANT_SAC}.
4. Perform optimization on the remaining OPC (τ_{AG_AC}, N_{AG_SAC}) across all pulse widths (PW_{AG}) for each saccade using NM to minimize the absolute positional error between the measured and simulated trajectory.
5. Select the 3 least-error OPC subsets for each saccade.
6. For each subject, fix τ_{AG_AC} to the mode of its least-error values.
7. Perform optimization on the remaining OPC (N_{AG_SAC}) across all pulse widths (PW_{AG}) for each saccade using NM to minimize the absolute positional error between the measured and simulated trajectory.
8. Select the 3 least-error OPC subsets for each saccade.
9. For each subject, perform exponential regression on the values of N_{AG_SAC}.
10. Calculate absolute positional error of the various OPC sets across all pulse widths (PW_{AG}) for each saccade.
11. Select the 3 least-error pulse width for each saccade.
12. Perform linear regression on the values of PW_{AG}.

4.5 Analysis

To evaluate the ability of the 2D-OP to simulate oblique saccades with properties resembling those of normal human saccades, RMSE and R^2 values were calculated to determine the accuracy of the 2D-OP in simulating positional signal, velocity signal, and main sequence relationships. To verify the robustness of OPC estimation, this process was repeated for saccade subsets of 0 – 10° amplitude and 0 – 15° amplitude. Recordings from the first experiment paradigm were employed for this analysis, as the stimulus provided highly stereotyped and stable saccades.

OPC estimation was repeated in several stages, with certain OPC being fixed to their average least-error value at each stage, with the goal of stabilizing constants first (e.g. K_{SE}, K_{LT}, B_P, J, etc.), followed by equations (e.g. N_{AG_SAC}, PW, etc.) ordered by increasing complexity. The output from each stage was provided as an input to the subsequent stage. At each stage, fixing certain OPC resulted in the formation of more stable and noticeable patterns in the values of the remaining OPC, allowing more accuracy in the resulting optimization and subsequent regression of parameter values. Several optimization techniques were considered and the heuristic presented in Algorithm 1 was selected because it produced OPC that allow the 2D-OP to simulate more accurate trajectories.

To evaluate the physiological accuracy of component parameters required for such application, we compare estimated model parameters from the first experiment paradigm to measured physiological ranges, where available. Obtaining physical measurements of these values requires surgery and informed consent in human subjects, and many candidates for such surgery elect to do so due to a physical abnormality that requires correction. As such there is a very small human subject pool from which to draw conclusions. In many cases, physiological measurements are estimated based on available information from humans, monkeys, and cats.

To evaluate the precision of parameters derived for person-specific saccades, we employ basic biometric techniques to differentiate individuals based on model parameters derived from the recordings of the second experiment paradigm. Pearson's correlation coefficient (Rodgers and Nicewander 1988) was averaged for each parameter across recording sessions to identify the consistency of parameter estimation between recording sessions. Hoteling's T-square test (Hotelling 1931) is utilized to compare sets of OPC vectors and return a similarity score used for acceptance or rejection of claimed identity. Information fusion of horizontal and vertical components is performed by a simple weighted mean of similarity scores, with weights selected to minimize equal error rate. False acceptance rate and false rejection rate were calculated across all acceptance thresholds, and equal error rate was used to determine the biometric viability of the technique (Jain, et al. 2007). Kolmogorov-Smirnov tests for normality and uniformity were applied to similarity scores to identify randomness (Massey 1951).

5. RESULTS

5.1 Saccade Simulation

RMSE is a measure of the difference between predicted and measured values, while the coefficient of determination, R^2, provides a measure of the degree to which predicted values follow measured values; according to (5) and (6), where m indicates a measured value, p indicates a predicted value, and n denotes the total number of data points:

$$RMSE = \frac{\sqrt{\left(\Sigma(m - p)^2\right)}}{n} \tag{5}$$

$$R^2 = \frac{(n\Sigma(m \times p) - \Sigma(m)\Sigma(p))^2}{(n\Sigma(m^2) - \Sigma(m)^2)\,(n\Sigma(p^2) - \Sigma(p)^2)} \tag{6}$$

Table 1 presents RMSE and R^2 correlation between measured and simulated saccade trajectories, Table 2 presents RMSE and R^2 correlation between measured and simulated saccade velocity, and Table 3 provides the average main sequence relationships and corresponding R^2 of regression for each oblique angle. Figures 5-7 provide examples of measured and simulated main sequence relationships from several subjects, where each line represents a different oblique angle. Figure 8-10 present examples of measured and simulated oblique saccade trajectories, and Figures 11-13 present the corresponding velocity profiles.

5.2 Physiological Accuracy

Model parameters P1 – P2 indicate variables in the equation for PW, according to (7). Percent difference is measured as the absolute difference in measured and simulated parameter values over the measured value, according to (8):

$$PW = P1 \times |A| + P2 \tag{7}$$

$$\text{Percent Difference} = |\text{Simulated} - \text{Measured}| \,/\, \text{Measured} \tag{8}$$

Table 4 presents known/measured parameter ranges, average OPC parameters across all subjects, and the percent difference for each parameter. Where available, measured human parameter ranges are given. In many cases where exact measurements of individual parameters are not possible, estimations and linear approximations of typically non-linear components may be provided.

When considering the neuronal control signal, N_{AG_SAC}, a strict comparison of parameters is impractical. The normal firing rate of abducens motor neurons during fixation is between (0 – 300] spikes/second, with firing rates not exceeding 750 spikes/second for horizontal saccades of 10° (Sparks 2002). A regression of N_{AG_SAC} values was performed across all subjects to provide an accurate representation of the average pulse height equations for horizontal and vertical saccade components, (9) and (10) respectively:

$$N_{AG\ SAC\ HORIZONTAL} = 340.2\ (1 - e^{-|A| / 17.7})\ \text{spikes/second} \tag{9}$$

$$N_{AG\_SAC\_VERTICAL} = 301.5\ (1 - e^{-|A| / 13.8})\ \text{spikes/second} \tag{10}$$

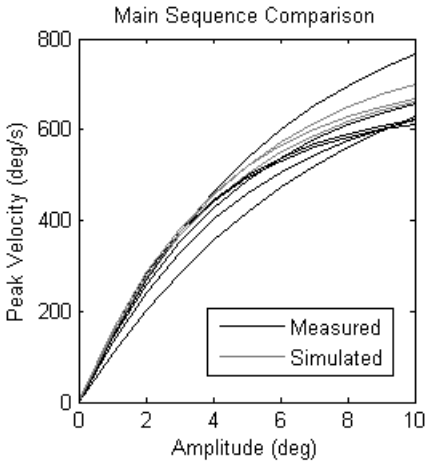

Figure 5. 0 – 10° amplitude, oblique main sequence, subject 8.

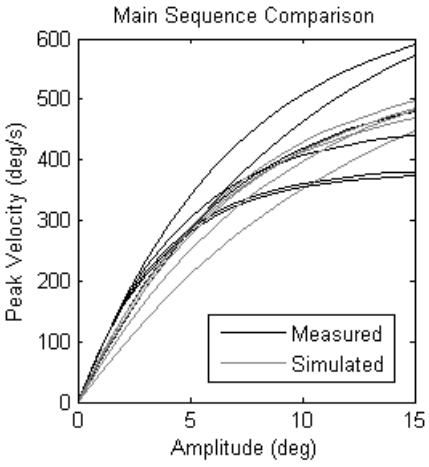

Figure 6. 0 – 15° amplitude, oblique main sequence, subject 24.

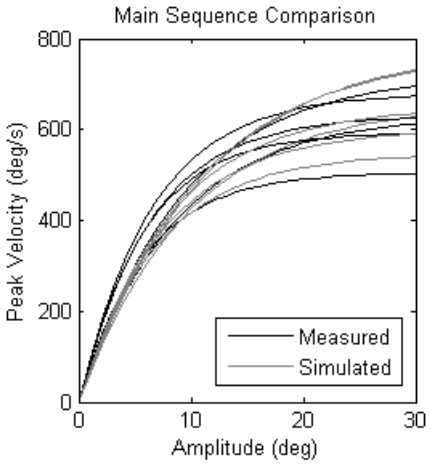

Figure 7. All saccades, oblique main sequence, subject 24.

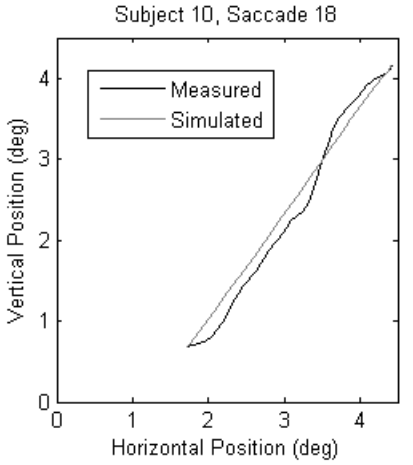

Figure 8. Comparative trajectory of a 3° saccade at a 45° angle.

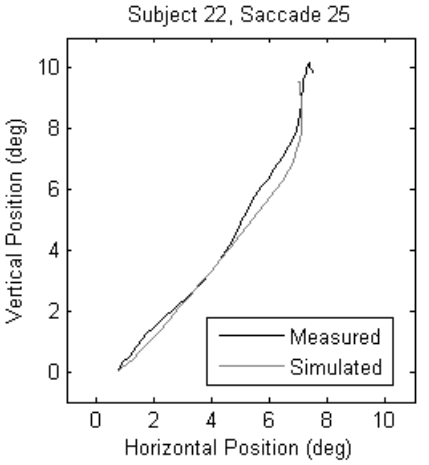

Figure 9. Comparative trajectory of a 12° saccade at a 60° angle.

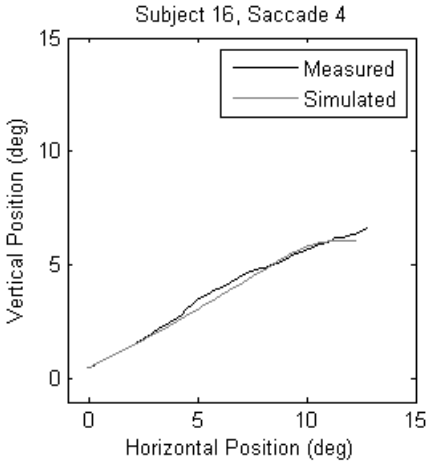

Figure 10. Comparative trajectory of a 15° saccade at a 30° angle.

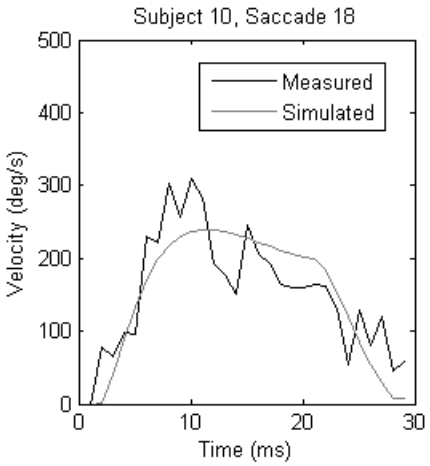

Figure 11. Comparative velocity of a 3° saccade at a 45° angle.

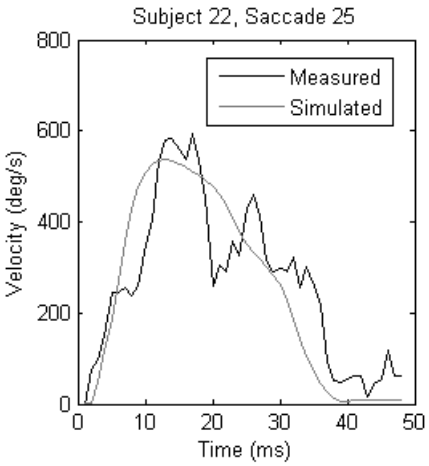

Figure 12. Comparative velocity of a 12° saccade at a 60° angle.

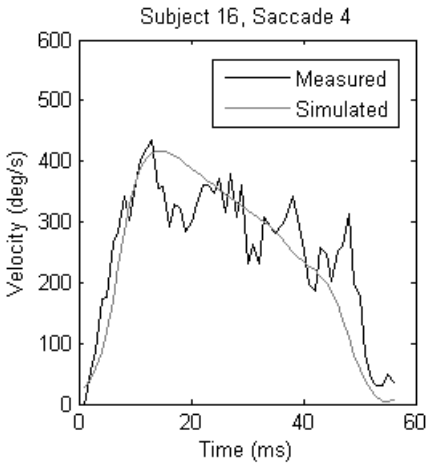

Figure 13. Comparative velocity of a 15° saccade at a 30° angle.

	0 – 10° Amplitude				*0 – 15° Amplitude*				*All Saccades*			
	RMSE		**R²**		**RMSE**		**R²**		**RMSE**		**R²**	
Component	**μ**	**σ**	**μ**	**σ**	**μ**	**σ**	**μ**	**σ**	**μ**	**σ**	**μ**	**σ**
Horizontal	0.63°	0.61°	0.83	0.25	0.72°	0.64°	0.85	0.25	0.81°	0.96°	0.86	0.24
Vertical	0.64°	0.58°	0.84	0.24	0.77°	0.82°	0.85	0.24	0.87°	0.96°	0.85	0.25
Oblique	0.64°	0.60°	0.84	0.25	0.75°	0.73°	0.85	0.24	0.84°	0.96°	0.85	0.24

Table 1. Positional Accuracy.

	0 – 10° Amplitude				*0 – 15° Amplitude*				*All Saccades*			
	RMSE		**R²**		**RMSE**		**R²**		**RMSE**		**R²**	
Component	**μ**	**σ**	**μ**	**σ**	**μ**	**σ**	**μ**	**σ**	**μ**	**σ**	**μ**	**σ**
Horizontal	98°/s	283°/s	0.47	0.29	103°/s	309°/s	0.49	0.29	116°/s	367°/s	0.51	0.29
Vertical	100°/s	287°/s	0.39	0.27	103°/s	272°/s	0.40	0.27	116°/s	333°/s	0.39	0.27
Oblique	118°/s	400°/s	0.55	0.26	124°/s	409°/s	0.59	0.25	141°/s	493°/s	0.59	0.25

Table 2. Velocity Accuracy.

	0 – 10° Amplitude											
	Measured						**Simulated**					
	V_{MAX}		**C**		**R²**		**V_{MAX}**		**C**		**R²**	
Angle	**μ**	**σ**	**μ**	**σ**	**μ**	**σ**	**μ**	**σ**	**μ**	**σ**	**μ**	**σ**
0°	539	38	4.32	0.59	0.94	0.06	519	22	5.17	3.10	0.99	0.02
15°	553	149	4.71	1.90	0.88	0.15	634	212	6.08	3.65	0.94	0.15
30°	542	125	4.55	1.66	0.81	0.16	572	137	5.85	1.73	0.96	0.09
45°	587	118	5.22	2.43	0.85	0.19	649	159	6.10	2.00	0.97	0.04
60°	601	223	5.51	3.32	0.75	0.32	584	171	6.24	2.03	0.96	0.06
75°	563	125	4.37	2.34	0.78	0.23	575	160	6.93	4.89	0.96	0.04
90°	586	112	4.75	1.20	0.82	0.14	358	29	4.27	1.11	0.98	0.02
	0 – 15° Amplitude											
	Measured						**Simulated**					
	V_{MAX}		**C**		**R²**		**V_{MAX}**		**C**		**R²**	
Angle	**μ**	**σ**	**μ**	**σ**	**μ**	**σ**	**μ**	**σ**	**μ**	**σ**	**μ**	**σ**
0°	597	128	5.37	1.92	0.79	0.25	630	156	9.33	2.94	0.94	0.07
15°	583	128	4.97	3.25	0.82	0.20	675	152	9.33	3.78	0.94	0.17
30°	627	129	5.38	2.32	0.84	0.14	654	161	8.01	3.17	0.95	0.05
45°	616	118	5.57	2.54	0.82	0.25	638	158	7.86	2.66	0.96	0.05
60°	590	175	4.99	2.79	0.59	0.38	579	150	7.19	2.37	0.95	0.06
75°	557	114	4.59	1.64	0.81	0.18	633	173	9.39	4.37	0.93	0.12
90°	619	149	6.28	2.43	0.78	0.20	611	319	8.06	5.26	0.99	0.01
	All Saccades											
	Measured						**Simulated**					
	V_{MAX}		**C**		**R²**		**V_{MAX}**		**C**		**R²**	
Angle	**μ**	**σ**	**μ**	**σ**	**μ**	**σ**	**μ**	**σ**	**μ**	**σ**	**μ**	**σ**
0°	584	108	5.56	1.65	0.82	0.24	633	121	10.38	3.43	0.95	0.07
15°	602	116	5.37	2.11	0.80	0.18	667	121	9.55	3.32	0.97	0.03
30°	625	95	5.94	3.05	0.84	0.14	649	155	8.28	3.26	0.95	0.05
45°	644	131	6.24	2.97	0.84	0.16	680	131	8.88	2.69	0.96	0.05
60°	615	179	5.16	2.71	0.59	0.35	606	165	8.81	3.79	0.94	0.09
75°	559	100	4.49	1.56	0.75	0.27	577	136	8.24	3.45	0.93	0.11
90°	624	152	6.33	2.52	0.76	0.20	447	91	6.03	1.73	0.89	0.23

Table 3. Measured and Simulated Oblique Main Sequences, $V_{PEAK} = V_{MAX}\ (1 - e^{-|Amplitude| / C})$

	Measured		*Simulated*					
			Horizontal			**Vertical**		
Parameter	**μ**	**Source**	**μ**	**σ**	**Difference**	**μ**	**σ**	**Difference**
K_{SE_AG}	2.5	(Collins 1975)	2.5	0.3	0%	2.3	0.3	8%
K_{SE_ANT}	2.5	(Collins 1975)	2.9	0.4	16%	2.6	0.4	4%
K_{LT_AG}	1.2	(Bahill 1980)	1.3	0.1	8%	1.3	0.1	8%
K_{LT_ANT}	1.2	(Bahill 1980)	1.4	0.1	17%	1.4	0.1	17%
K_P	0.5	(Collins 1975)	0.4	0.1	20%	0.4	0.0	20%
B_P	0.06	(Bahill, et al. 1980)	0.040	0.007	33%	0.043	0.007	28%
B_{AG}	0.046	(Bahill, et al. 1980)	0.040	0.004	13%	0.041	0.004	11%
B_{ANT}	0.022	(Bahill, et al. 1980)	0.017	0.003	23%	0.019	0.003	14%
J	$4.3(10^{-5})$	(Bahill, et al. 1980)	$4.9(10^{-5})$	$0.8(10^{-5})$	14%	$5.4(10^{-5})$	$0.6(10^{-5})$	26%
τ_{AG_AC}	9.7*	(Bahill, et al. 1980)	1.5	0.0	85%	1.5	0.0	85%
τ_{ANT_AC}	2.0	(Hsu, et al. 1976)	3.1	0.2	55%	3.0	0.2	50%
τ_{AG_DE}	2.4	(Bahill, et al. 1980)	2.4	0.1	0%	2.4	0.1	0%
τ_{ANT_DE}	1.9	(Bahill, et al. 1980)	2.1	0.1	11%	2.2	0.1	16%
N_{FIX_C}	14	(Bahill 1980)	15.9	1.4	14%	14.6	1.6	4%
N_{ANT_SAC}	0.8	(Bahill 1980)	0.51	0.02	36%	0.51	0.03	36%
P1	1.0	(Collins 1975)	1.7	0.6	70%	1.7	0.8	70%
P2	10.0	(Collins 1975)	2.3	4.3	77%	1.6	3.0	84%

* Based on referenced estimation for 10° saccades.

Table 4. Estimated Oculomotor Plant Characteristics.

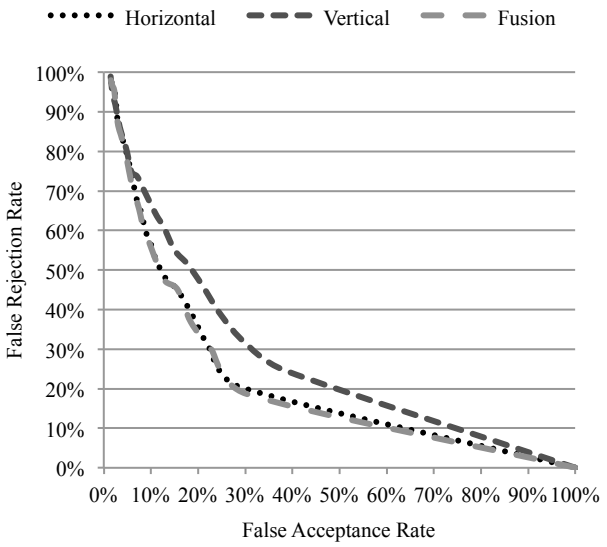

Figure 14. Detection Error Tradeoff (DET) Curve.

Parameter	Horizontal		Vertical	
	r	p	r	p
K_{SE_AG}	0.0000	0.5084	0.0006	0.4869
K_{SE_ANT}	0.0006	0.4962	0.0015	0.4961
K_{LT_AG}	0.0006	0.5013	0.0019	0.5084
K_{LT_ANT}	-0.0009	0.4989	-0.0006	0.5133
N_{AG_C}	0.0010	0.4997	0.0019	0.4914
N_{ANT_C}	0.0002	0.4993	-0.0004	0.4976
B_P	-0.0005	0.4974	-0.0016	0.5019
B_{AG}	-0.0006	0.4984	0.0012	0.4929
B_{ANT}	-0.0004	0.4995	-0.0016	0.4917
J	0.0006	0.5040	-0.0019	0.4899
τ_{AG_AC}	0.0003	0.4942	0.0005	0.5075
τ_{ANT_AC}	-0.0000	0.5019	0.0003	0.5221
τ_{AG_DE}	0.0018	0.5008	-0.0011	0.4997
τ_{ANT_DE}	-0.0011	0.5079	0.0002	0.5132
N_{FIX_C}	0.0018	0.5083	-0.0006	0.5009
N_{AG_SAC}	-0.0014	0.5052	-0.0003	0.5078
N_{ANT_SAC}	-0.0003	0.5002	-0.0011	0.4962
PW	-0.0015	0.5051	0.0003	0.4989

Table V. Pearson's Correlation Coefficient.

5.3 Physiological Precision

False acceptance rate (FAR) is defined as the rate at which unauthorized individuals are accepted by a biometric authentication system as valid users, while false rejection rate (FRR) is defined as the rate at which authorized individuals are rejected by the system as invalid users. The detection error tradeoff (DET) curve, shown in Figure 14, plots false acceptance rate against false rejection rate at varied acceptance thresholds. The horizontal component provided an equal error rate of 25.98%, the vertical component provided an equal error rate of 30.79%, with fusion providing an equal error rate of 25.02%, using the following weighting: 0.95 × Horizontal + 0.05 × Vertical.

Kolmogorov-Smirnov tests for normality (D = 0.5000, p = 0.0000) and uniformity (D = 0.6311, p = 0.0000) of fused similarity scores generated by Hoteling's T-square comparisons of OPC parameters rejected the possibility that similarity scores conform to either distribution. Pearson's correlation coefficient was averaged for each parameter across recording sessions to identify the consistency of parameter estimation between recording sessions, with test statistics reported in Table 5.

6. DISCUSSION

The model achieves fair accuracy in the simulation of saccades with characteristics resembling those of normal humans. The results of our estimation indicate that, during expansion and stretching, components act slightly differently (similar to differences in force-velocity relationships). It is very easy to detect when a component is part of the agonist or antagonist. Therefore, breaking those components into agonist and antagonist counterparts increases the accuracy of the model while keeping the complexity linear. With the exception of N_{AG_SAC}, estimated OPC parameters are relatively consistent across the considered intervals (generally varying by less than 10% in both mean and standard deviation) and fall within a degree of magnitude from their initial values. High variability in the values of N_{AG_SAC} is likely due to major oversimplification of the neural processes that interact to produce muscle innervation, reducing an even more complex, interactive system to a single equation without accounting for non-linear interactions that may occur at the neural level during pulse generation.

The positional error of simulated saccades was small (0.63-0.87° on average). As the range of saccades included in OPC estimation increases, both RMSE and R^2 of the simulated trajectory increase. That is, as the data set increases, the average positional error of simulated saccades increases, but the average correlation between measured and simulated saccades also increases. This is likely due to the inclusion of greater amplitude saccades, which contribute relatively more error to the RMSE calculation. Such error might occur due to the linear representation of the OP by the 2D-OP model, as the linear representation is more accurate toward the primary eye position.

The accuracy of velocity simulation is similar to that of the positional accuracy, as the range of saccades included in OPC estimation increases, both RMSE and R^2 increase. In addition, it should be noted that the ratio of peak velocity to average velocity (Q) of measured saccades had an average value of 2.74 (SD = 3.02), while the simulated Q had an average value of 2.01 (SD = 0.66).

The main sequence relationship for the oblique angles of each subject was calculated separately based on the available data for both measured and simulated saccades. In some cases, insufficient data for a given angle and outliers resulted in unusable fits. To mediate the effect of including this data in the average, relationships were excluded based on the following criteria: regression failed for a given data set; R^2 of the regression was negative; V_{MAX} was unrealistically high (>1000°/s). Because of this exclusion, the averaged value for each angle was not necessarily drawn from the average data across all subjects, but only a subset of this. Of the oblique angles, 0° and 90° tended to have the most data loss in this respect. This occurs because purely horizontal/vertical saccades are very rare, and even when the eye is programmed for such a saccade, there is a certain amount of drift that occurs in the orthogonal component, resulting in a skewed oblique angle.

As expected from the literature, the simulated values of V_{MAX} produced for all angles (358 ~ 680°/s) are within a realistic range (400 ~ 800°/s), as is the curvature. The average R^2 for regressions of measured saccades are often lower than the average R^2 for simulated saccades, suggesting that the model provides a stricter adherence to the main sequence relationship than is found in normal human saccades, possibly due to noise or measurement inaccuracy.

The physiological accuracy of model parameters is tentatively confirmed to fall within normal human ranges, due primarily to the relatively low availability of measurable human data. With the exception of activation time constants and neural pulse width, all estimated model parameters are relatively close to measured values, and the neuronal control signal falls within a realistic output of spikes/second, well below measured limitations. A constant with initial value 0.5 was assigned to N_{ANT_SAC} based on early experiments with parameter estimation that showed that N_{ANT_SAC} assumes a non-zero value at saccades of low amplitude and rapidly decreases in an asymptotic manner, approaching zero as saccade amplitude increases.

The precision of model parameters and parameter estimation is largely confirmed by the results of biometric analysis. Pearson's correlation coefficient failed to identify linear dependence or independence of parameter estimation between sessions. This is not entirely unexpected, as parameter estimation is performed across a large number of variables using a local minimization algorithm. The Kolmogorov-Smirnov tests for normality ($p = 0.00$) and uniformity ($p = 0.00$) indicate that the similarity scores generated by Hoteling's T-square are non-random, and the equal error rate of 25.02% indicates that OPC parameters constitute viable biometric indicators, far from the chance value of 50%. It should be noted that, in biometric applications, fatigued or otherwise abnormal saccades would be treated in the same manner as smudged fingerprints. While OPC parameters do not present enough biometric accuracy to replace existing biometric authentication methods (possibly due to the linear nature of the model, or inaccuracy in parameter estimation), the OPC is immediately applicable as a component of multi-biometric systems. In a related study (Komogortsev, et al. 2012a), the combination of iris recognition, OPC parameters, and eye movement analysis in an ocular multi-biometric system reduced error by 13.4% over purely iris recognition-based authentication, for an equal error rate of 4.8%.

7. CONCLUSION

To assess the performance of the two-dimensional linear homeomorphic oculomotor plant mathematical model, approximately 1200 centrifugal oblique saccades and 12000 uniformly random oblique saccades were recorded from 30 human subjects. The results suggest that the two-dimensional linear homeomorphic oculomotor plant mathematical model is capable of simulating saccadic eye movements with characteristics resembling those of normal humans, with model parameters within feasible physiological ranges, and with parameter estimation precise enough to uniquely identify individuals based solely on estimated model parameters.

The most accurate simulation results were obtained for saccades with amplitudes between 0-10° amplitude; however, larger saccades were simulated relatively accurately, with average positional error not exceeding 0.87° and 141°/s respectively. Oblique main sequences generated by the two-dimensional linear homeomorphic oculomotor plant mathematical model resulted in a better fit to the stereotyped exponential form than recorded human data. As well, biometric application of the oculomotor plant model yielded an equal error rate of 25.02%, far from the random chance value of 50%, with Kolmogorov-Smirnov tests confirming non-random distribution of biometric match scores.

The results indicate that the model is capable of producing oblique saccades with properties resembling those of normal human saccades, and is capable of deriving muscle constants that are viable as biometric indicators. Therefore, we conclude that sacrifice in the anatomical accuracy of the model produces negligible effects on the accuracy of saccadic simulation on a 2D plane, and may provide a usable model for applications in computer science, human-computer interaction, and related fields.

REFERENCES

Bahill. 1980. Development, Validation, and Sensitivity Analyses of Human Eye Movement Models. *Critical Reviews in Bioengineering* 4, 4, 311-355.

Bahill, Clark and Stark. 1975. The Main Sequence, A Tool for Studying Human Eye Movements. *Mathematical Biosciences* 24, 3-4, 191-204.

Bahill, Latimer and Troost. 1980. Linear Homeomorphic Model for Human Movement. *IEEE Transactions on Biomedical Engineering* 27, 11, 631-639.

Bahill and Stark. 1977. Oblique Saccadic Eye Movements: Independence of Horizontal and Vertical Channels. *Archives of Ophthalmology* 95, 7, 1258-1261.

Carpenter. 1977. *Movements of the Eyes*. *Pion Ltd*,

Ciuffreda and Stark. 1975. Descartes' Law of Reciprocal Innervation. *American Journal of Optometry & Physiological Optics* 52, 10, 663-673.

Clark and Stark. 1974. Control of Human Eye Movements: I. Modelling of Extraocular Muscles; II. A Model for the Extraocular Plant Mechanism; III. Dynamic Characteristics of the Eye Tracking Mechanism. *Mathematical Biosciences* 20, 3-4, 191-265.

Collins. 1975. The Human Oculomotor Control System.

Enderle, Engelken and Stiles. 1991. A Comparison of Static and Dynamic Characteristics Between Rectus Eye Muscle and Linear Muscle Model Predictions. *IEEE Transactions on Biomedical Engineering* 38, 12, 1235-1245.

Enderle and Zhou. 2010. *Models of Horizontal Eye Movements, Part II: A 3rd Order Linear Saccade Model*. *Morgan & Claypool Publishers*,

SR Research. EyeLink 1000 Eye Tracker. Available: http://www.sr-research.com/.

Fioravanti, Inchingolo, Pensiero and Spanio. 1995. Saccadic Eye Movement Conjugation in Children. *Vision Research* 35, 23-24, 3217-3228.

Harwood and Herman. 2008. Optimally Straight and Optimally Curved Saccades. *The Journal of Neuroscience* 28, 30, 7455-7457.

Hotelling. 1931. The Generalization of Student's Ratio. *The Annals of Mathematical Statistics* 2, 3, 360-378.

Hsu, Bahill and Stark. 1976. Parametric Sensitivity Analysis of a Homeomorphic Model for Saccadic and Vergence Eye Movements. *Computer Programs in Biomedicine* 6, 108-116.

Huaman and Sharpe. 1993. Vertical Saccades in Senescence. *Investigative Ophthalmology & Visual Science* 34, 8, 2588-2595.

Jain, Flynn and Ross. 2007. Handbook of Biometrics.

Komogortsev. 2007. Eye Movement Prediction by Oculomotor Plant Modeling with Kalman Filter.

Komogortsev, Gobert, Jayarathna, Koh and Gowda. 2010. Standardization of Automated Analyses of Oculomotor Fixation and Saccadic Behaviors. *IEEE Transactions on Biomedical Engineering* 57, 11, 2635-2645.

Komogortsev, Karpov, Holland and Proença. 2012a. Multimodal Ocular Biometrics Approach: A Feasibility Study.

Komogortsev, Karpov, Price and Aragon. 2012b. Biometric Authentication via Oculomotor Plant Characteristics.

Komogortsev and Khan. 2007. Perceptual Multimedia Compression Based on Predictive Kalman Filter Eye Movement Modeling.

Komogortsev and Khan. 2008. Eye Movement Prediction by Kalman Filter with Integrated Linear Horizontal Oculomotor Plant Mechanical Model.

Komogortsev and Khan. 2009. Eye Movement Prediction by Oculomotor Plant Kalman Filter with Brainstem Control. *Journal of Control Theory and Applications* 7, 1, 14-22.

Komogortsev, Ryu, Koh and Gowda. 2009. Instantaneous Saccade Driven Eye Gaze Interaction.

Lagarias, Reeds, Wright and Wright. 1998. Convergence Properties of the Nelder-Mead Simplex Method in Low Dimensions. *SIAM Journal of Optimization* 9, 1, 112-147.

Leigh and Zee. 2006. *The Neurology of Eye Movements*. *Oxford University Press*, Oxford, NY, USA.

Martin and Schovanec. 1998. Muscle Mechanics and Dynamics of Ocular Motion. *Journal of Mathematical Systems, Estimation, and Control* 8, 2, 1-15.

Massey. 1951. The Kolmogorov-Smirnov Test for Goodness of Fit. *Journal of the American Statistical Association* 46, 253, 68-78.

Pelisson and Prablanc. 1988. Kinematics of Centrifugal and Centripetal Saccadic Eye Movements in Man. *Vision Research* 28, 1, 87-94.

Quaia and Optican. 2003. Dynamic Eye Plant Models and the Control of Eye Movements. *Strabismus* 11, 1, 17-31.

Quaia, Ying and Optican. 2010. The Viscoelastic Properties of Passive Eye Muscle in Primates. III: Force Elicited by Natural Elongations. *PLoS ONE* 5, 3, 1-19.

Robinson. 1973. Models of the Saccadic Eye Movement Control System. *Biological Cybernetics* 14, 2, 71-83.

Rodgers and Nicewander. 1988. Thirteen Ways to Look at the Correlation Coefficient. *The American Statistician* 42, 1, 59-66.

Sparks. 2002. The Brainstem Control of Saccadic Eye Movements. *Nature Reviews: Neuroscience* 3, 952-964.

Tamir, Komogortsev and Mueller. 2008. An Effort and Time Based Measure of Usability.

Tweed and Vilis. 1987. Implications of Rotational Kinematics for the Oculomotor System in Three Dimensions. *Journal of Neurophysiology* 58, 4, 832-849.

Westheimer. 1954. Mechanism of Saccadic Eye Movements. *Archives of Ophthalmology* 52, 710-723.

Yee, Schiller, Lim, Baloh, Baloh and Honrubia. 1985. Velocities of Vertical Saccades with Different Eye Movement Recording Methods. *Investigative Ophthalmology & Visual Science* 26, 7, 938-944.